

# Observation of charge carrier localization-induced negative magnetoresistance at room temperature in helium-ion-irradiated defective graphene

Takuya Iwasaki<sup>1\*</sup>, Shu Nakamura<sup>2</sup>, Osazuwa Gabriel Agbonlahor<sup>2</sup>, Manoharan Muruganathan<sup>2</sup>, Masashi Akabori<sup>2</sup>, Yoshifumi Morita<sup>3</sup>, Satoshi Moriyama<sup>1</sup>, Shinichi Ogawa<sup>4</sup>, Yutaka Wakayama<sup>1</sup>, Hiroshi Mizuta<sup>2,5</sup> and Shu Nakaharai<sup>1</sup>

<sup>1</sup> NIMS, 1-1 Namiki, Tsukuba, Ibaraki 305-0044, Japan

<sup>2</sup> JAIST, 1-1 Asahidai, Nomi, Ishikawa 923-1292, Japan

<sup>3</sup> Gunma Univ., Kiryu, Gunma 376-8515, Japan

<sup>4</sup> AIST, 1-1-1 Umezono, Tsukuba, Ibaraki 305-8560, Japan

<sup>5</sup> Hitachi Camb. Lab., J. J. Thomson Avenue, Cambridge CB3 0HE, UK

\*Phone: +81(0)29-851-3354 (ext. 8670), E-mail: IWASAKI.Takuya@nims.go.jp

## Abstract

We systematically investigate the magnetotransport of He-ion-irradiated graphene, where negative magnetoresistance due to strong localization-dominated hopping transport is observed. By tuning device parameters for certain conditions, the negative magnetoresistance persists up to room temperature, first revealed for graphene devices. Our study clarifies carrier localization via search in the multi-dimensional parameter space of Dirac materials, leading to a deep understanding of Anderson localization physics, and to defect engineering for two-dimensional material-based electromagnetic device applications.

## 1. Introduction

Anderson localization (AL), a major theme of condensed matter physics, has been studied for more than half a century. Since the discovery of graphene, its unique AL in Dirac materials, particularly weak localization, has been studied intensively [1]. Strong localization (SL) has also been investigated in graphene with intentionally introduced defects [2–4]. In the SL regime, the electrical conductance is determined by hopping transport between localized states. The time-reversal symmetry breaking due to, for example, the application of a magnetic field leads to destructive interference and orbital effects between the localized states, which can increase the hopping probability [5,6]. This results in the conductance increase, i.e., negative magnetoresistance (MR).

Thus far, defects were introduced into graphene by oxidation with ozone exposure [2], Ga-ion-irradiation using a focused ion beam [3], and hydrogenation [4]. In these defective graphene systems, SL properties, such as negative MR and two-dimensional (2D) variable-range hopping (VRH), have been reported. These effects can be seen only at extremely low temperatures in conventional 2D thin-film materials [5,6]. Although the precise control of spacing/strength of defects using conventional methods is challenging, the He-ion-irradiation method using an ion microscope is a promising technology, by which the point defect density in graphene can be controlled by tuning the ion dose [7]. However, the MR of He-ion-irradiated graphene has been unexplored so far.

In this study, we investigate the transport properties of

He-ion-irradiated graphene systematically. The properties include its dependence on the magnetic field, temperature, channel size, carrier density, and ion dose.

## 2. Methods

The device schematic and an optical image of the typical device used in this study are shown in Fig. 1. Monolayer graphene devices were fabricated by the conventional process. We defined the effective channel as the region between Cr/Au electrodes with controlled mild dose irradiation. Other regions were insulated by irradiation with a high dose of  $\sim 1.3 \times 10^{16}$  ions/cm<sup>2</sup> [7]. The electrode width ( $W_e$ ) and the non-insulating region width ( $W$ ) are almost equal, and the effective channel length ( $L$ ) and the distance between the electrodes ( $L_{gap}$ ) are almost the same. This is designed to minimize the contribution from non-irradiated graphene regions and to prevent damage at the interface between the graphene and the electrode. Note that  $W$  is designed  $\geq 200$  nm to avoid the influence of edge disorder.

For ion irradiation, a focused He ion beam was irradiated onto graphene using an ion microscope (Zeiss Orion Plus) with the acceleration voltage of 30 kV.

The devices were measured in a <sup>4</sup>He cryostat equipped with a variable temperature insert for the temperature ( $T$ ) range of 10–300 K. Using a superconducting magnet, a magnetic field ( $B$ ) up to 6 T was applied perpendicularly to the substrate. For the electrical resistance measurement, the source-drain bias voltage ( $V_{sd}$ ) was applied, and the drain current ( $I_d$ ) was measured in a two-terminal DC configuration. The gate voltage ( $V_g$ ) was applied to the Si substrate.

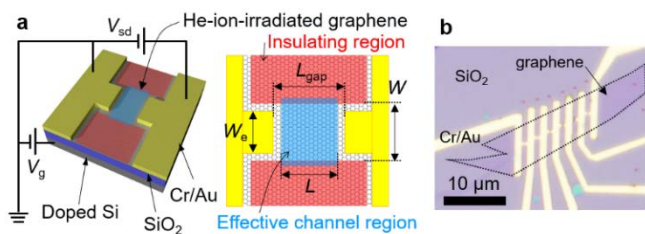


Fig. 1. (a) Schematic of the device structure and the measurement configuration. (b) Optical image of the typical device used in this study. The dotted line indicates the edge of graphene.

### 3. Results and Discussion

We investigated the 23 devices with various parameters and obtained consistent results. Here, we focus on the device with  $L = W = 1.0 \mu\text{m}$  and a dose of  $0.5 \times 10^{15} \text{ ions/cm}^2$ . The MR ( $\Delta R/R_0$ ) vs.  $B$  at  $V_g$  of the charge neutral point (CNP) is plotted in Fig. 2a, where  $R_0 = R(B=0) = V_{sd}/I_d(B=0)$  and  $\Delta R = R(B) - R_0$ . The negative MR is observed in the entire  $T$  range up to 300 K. The absolute MR value  $|\Delta R/R_0|$  increases with  $B$  and is not saturated even at  $B = 6 \text{ T}$ . Figure 2b shows the MR vs.  $B$  plot at  $T = 10 \text{ K}$  for each hole density ( $n_h$ ) which is derived by the geometrical capacitance model. The  $|\Delta R/R_0|$  is maximized at the CNP to be  $-0.51$  at  $B = 6 \text{ T}$ .

In the SL regime, the transport mechanism including magnetotransport is dominated by the 2D-VRH, in which the  $T$ -dependence of  $R$  is described by  $R \sim \exp[(T_0/T)^{1/3}]$ . Here,  $T_0$  is the characteristic temperature of VRH, expressed as  $T_0 = 3/(k_B N(E)\zeta^2)$ , where  $k_B$  is the Boltzmann constant,  $N(E)$  the density of states (DoS) at energy  $E$ , and  $\zeta$  the localization length [8]. These characteristics can be confirmed in our devices, as shown in the  $R$  vs.  $T^{-1/3}$  semi-log plot (Fig. 2c). By applying the DoS at the Fermi energy, we estimate  $\zeta$  to be  $\sim 24, 21$ , and  $25 \text{ nm}$  for  $n_h = 0.8, 1.5$ , and  $2.3 \times 10^{12} \text{ cm}^{-2}$ , respectively. This indicates that  $|\Delta R/R_0|$  can be modulated by  $n_h$  via the DoS variation, whereas  $\zeta$  is not largely changed.

The SL interference effects also contribute to the magnetoconductance as  $\Delta G/G_0 \propto B^2$  (where  $G_0 = G(B=0)$ ,  $\Delta G = G(B) - G_0$ ) [5,6]. This property is observed as shown in the Fig. 2d. Moreover, we find  $\Delta G/G_0 \propto T^\beta$  with  $\beta \sim 1.2$  [9]. These properties are consistent with those of other systems in the SL regime [5,6,9], indicating that 2D-VRH in the SL regime is the dominant transport mechanism in our devices.

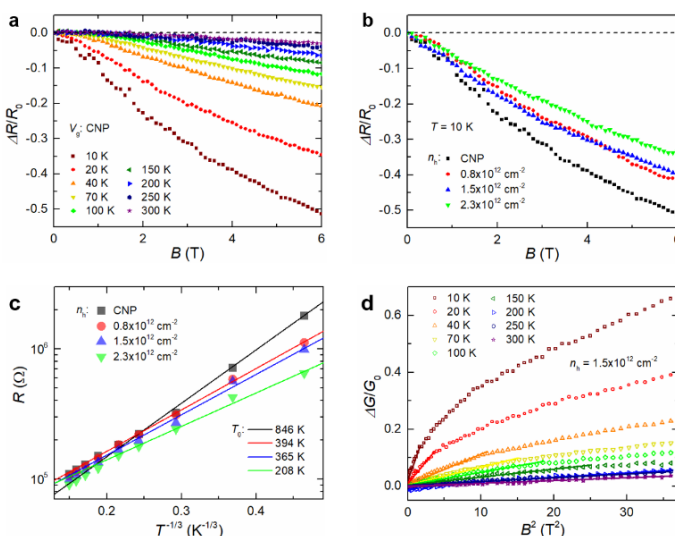


Fig. 2. Transport properties of the device with  $L = W = 1.0 \mu\text{m}$  and a dose of  $0.5 \times 10^{15} \text{ ions/cm}^2$ . (a)  $\Delta R/R_0$  vs.  $B$  plot at the CNP for various  $T$ .  $V_{sd}$  is fixed to 30 mV. (b)  $\Delta R/R_0$  vs.  $B$  plot at  $T = 10 \text{ K}$  for various  $n_h$ . (c)  $R$  vs.  $T^{-1/3}$  semi-log plot. The symbols represent the experimental data. The solid lines and  $T_0$  values are the fitting results with  $R \sim \exp[(T_0/T)^{1/3}]$ . (d)  $\Delta G/G_0$  vs.  $B^2$  plot at  $n_h = 1.5 \times 10^{12} \text{ cm}^{-2}$ . The symbols represent the experimental data. The solid lines represent the linear fitting result.

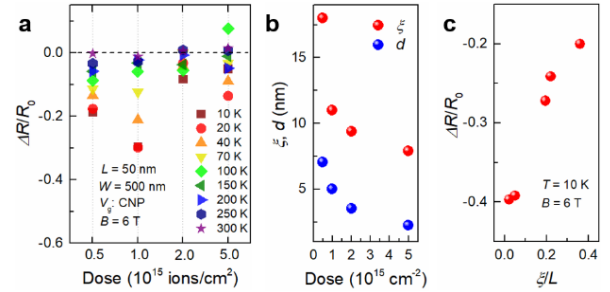


Fig. 3. (a)  $\Delta R/R_0$  at the CNP, at various  $T$  for doses of  $0.5, 1.0, 2.0$ , and  $1.0 \times 10^{15} \text{ ions/cm}^2$ .  $L = 50 \text{ nm}$ ,  $W = 500 \text{ nm}$ . (b) Dose dependence of  $\zeta$  and  $d$ . (c)  $\Delta R/R_0$  at  $T = 10 \text{ K}$ ,  $B = 6 \text{ T}$  as a function of  $\zeta/L$ .

Next, we examine the dose dependence of the MR by employing the devices for various doses with fixed  $L = 50 \text{ nm}$  and  $W = 500 \text{ nm}$ . Figure 3a displays  $\Delta R/R_0$  at the CNP and  $B = 6 \text{ T}$  for doses of  $0.5, 1.0, 2.0$ , and  $5.0 \times 10^{15} \text{ ions/cm}^2$ .

From the VRH fitting analysis, it is found that  $\zeta$  decreases with increasing the dose (Fig. 3b). The reason for this modulation could be associated with an average interval distance ( $d$ ) between point defects, which can be derived as  $d [\text{nm}] = (2.5 \times 10^{16}/\text{Dose} [\text{ions/cm}^2])^{1/2}$ . In fact,  $\zeta$  and  $d$  are obviously correlated (Fig. 3b). The high dose results in smaller/unstable  $|\Delta R/R_0|$ , which could be ascribed to small  $\zeta$  and  $d$ . Closing the carbon atom distance in graphene and  $d$  could lead to large defect formation due to point defect percolations, which can destroy graphene crystalline integrity and the interference effect. Figure 3c shows the  $\zeta/L$ -dependence of  $|\Delta R/R_0|$  at  $T = 10 \text{ K}$ ,  $B = 6 \text{ T}$ . This indicates that  $|\Delta R/R_0|$  increases with decreasing  $\zeta/L$ . Therefore,  $\zeta/L$  should be tuned to optimize  $|\Delta R/R_0|$ .

### 4. Conclusions

Magnetotransport properties of He-ion-irradiated graphene are investigated. The transport mechanism in He-ion-irradiated graphene is found to be SL-dominated 2D-VRH, and the MR can be modulated by the dose. Via a systematic parameter search in Dirac materials, negative MR is first revealed at room temperature by adopting He-ion-irradiation, which contrasts previous defective graphene devices [2–4].

### Acknowledgements

The authors thank H. Osato, E. Watanabe, and D. Tsuya from the NIMS Nanofabrication platform for assisting with the device fabrication. We acknowledge T. Iijima and Yukinori Morita from the AIST SCR Station for the usage of the He-ion microscope. This work was partially supported by JSPS KAKENHI 19K15385, 19H05520, 20K20442 and by NIMS Nanofabrication Platform in Nanotechnology Platform Project, WPI-MANA, sponsored by the MEXT, Japan. S.M. acknowledges financial support from the Murata Science Foundation.

### References

- [1] S. V. Morozov et al., Phys. Rev. Lett. **97**, 016801 (2006).
- [2] J. Moser et al., Phys. Rev. B **81**, 205445 (2010).
- [3] Y.-B. Zhou et al., Appl. Phys. Lett. **98**, 222502 (2011).
- [4] B. R. Matis et al., Phys. Rev. B **85**, 195437 (2012).
- [5] O. Entin-Wohlman et al., Phys. Rev. B **40**, 8342 (1989).
- [6] S.-Y. Hsu and J. M. Valles Jr., Phys. Rev. Lett. **74**, 2331 (1995).
- [7] S. Nakaharai et al., ACS Nano **7**, 5694 (2013).
- [8] N. F. Mott and G. A. Davis, *Electronic Processes in Non-Crystalline Materials*, 2nd ed. (Clarendon, Oxford, 1979).
- [9] Y. Zhang and M. P. Sarachik, Phys. Rev. B **43**, 7212 (1991).